Fluid simulation of the pulsed bias effect on inductively coupled nitrogen discharges for low-voltage plasma immersion ion implantation*

Xiao-Yan Sun(孙晓艳), Yu-Ru Zhang(张钰如), Xue-Chun Li(李雪春), and You-Nian Wang(王友年)†

Key Laboratory of Materials Modification by Laser, Ion, and Electron Beams (Ministry of Education), School of Physics and Optoelectronic Technology, Dalian University of Technology, Dalian 116024, *China*

(Received 23 July 2016; revised manuscript received 1 September 2016; published online 29 November 2016)

Planar radio frequency inductively coupled plasmas (ICP) are employed for low-voltage ion implantation processes, with capacitive pulse biasing of the substrate for modulation of the ion energy. In this work, a two-dimensional (2D) self-consistent fluid model has been employed to investigate the influence of the pulsed bias power on the nitrogen plasmas for various bias voltages and pulse frequencies. The results indicate that the plasma density as well as the inductive power density increase significantly when the bias voltage varies from 0 V to −4000 V, due to the heating of the capacitive field caused by the bias power. The N^+ fraction increases rapidly to a maximum at the beginning of the power-on time, and then it decreases and reaches the steady state at the end of the glow period. Moreover, it increases with the bias voltage during the power-on time, whereas the N_2^+ fraction exhibits a reverse behavior. When the pulse frequency increases to 25 kHz and 40 kHz, the plasma steady state cannot be obtained, and a rapid decrease of the ion density at the substrate surface at the beginning of the glow period is observed.

Keywords: fluid simulation, low-voltage plasma immersion ion implantation, N_2 inductive discharge

PACS: 52.30. Ex, 52.65.–y, 52.50.Qt **DOI:** 10.1088/1674-1056/26/1/015201

1. Introduction

The low-voltage plasma immersion ion implantation (LPIII), which is characterized by low energy and high throughput, has been widely used in the semiconductor industry, e.g., for changing the surface chemistry and surface morphology of silicone,[1] fabricating shallow junctions,[2–5] as well as improving the microhardness and reducing the friction coefficient and wear rate of stainless-steel surfaces.[6,7]

Since the chemical structure of the surface is changed after a nitrogen treatment, nitrogen has been widely applied in the LPIII process.[1,5,8–10] For instance, Husein *et al.*[1] demonstrated that the surface chemistry of the silicon, i.e., the formation of SiO_x, silicon oxynitrides and silicon nitrides, was changed after a nitrogen PIII treatment. Mukherjee *et al.*[8] revealed an enhancement of the surface microhardness, by implantation of the nitrogen in AISI 316 austenitic stainless steel. Moreover, Felch *et al.*[5] found that performing nitrogen plasma doping (PLAD) before ultra-low energy B^+ implantation, could reduce boron diffusion and produce shallower junctions.

Several pieces of equipment for LPIII have been proposed, for instance, the hot filament glow discharge configuration, the pulse- or direct current (DC)-biased electron cyclotron resonance (ECR) equipment, the pulse- or DC-biased ICP system, and so on.[7,11–17] In a pulse-biased ICP, a continuous inductive source is used to sustain the discharge, and a pulsed bias power is applied to the substrate to control the ion energy. Since this system offers higher ion densities at lower pressure, and the ion energy can be easily modulated by adjusting the bias power, the pulse-biased ICP has attracted growing interest.

Over the past few years, several theoretical studies[18,19] and experimental researches[1,15,16,20] have been published on a pulse-biased ICP. Agarwal *et al.*[18] applied a 2D hybrid model, and they found that the time averaged ion energy angular distribution (IEAD) was characterized by multi-energy structures, due to the contributions of the ions arriving during the pulse-on period (high energy) and the pulse-off period (low energy). Moreover, by using the same model, they revealed that the IEAD became asymmetric as the bias voltage increased from −1 kV to −10 kV, with the ICP power of 500 W.[19] Husein *et al.*[1] experimentally observed a rough silicon surface with deeper valleys during the PIII modification in N_2 plasmas, when the bias voltage was low (i.e., 4 kV). In addition, Qin *et al.*[15] focused on the PLAD process in a pulsed radio frequency (RF)-excited B_2H_6/H_2 plasma system, revealing that a deeper boron profile was produced, and the boron surface deposition decreased slightly at higher voltage. Subsequently, by using a time-delayed, time-resolved Langmuir probe, the higher plasma density and electron temperature were obtained in a continuous plasma with pulsed voltage

*Project supported by the National Natural Science Foundation of China (Grant Nos. 11175034, 11335004, and 11405019) and the Important National Science and Technology Specific Project of China (Grant No. 2011 ZX 02403-001).

†Corresponding author. E-mail: ynwang@dlut.edu.cn

© 2017 Chinese Physical Society and IOP Publishing Ltd

than in a non-continuous plasma.[16] Chang *et al*.[20] achieved the liquid crystal (LC) alignment on the hydrogenated amorphous carbon (a-C:H) layer by an argon plasma ion immersion treatment. They attributed the formation of the LC alignment to the oblique incidence of the ions within the matrix sheath of non-uniform thickness near the a-C:H surface under a negative pulse bias.

From the literature mentioned above, it is clear that the bias power has a significant influence on the plasma properties in a pulse-biased ICP. Therefore, the bias effect should be systematically investigated, in order to understand the discharge characteristics and optimize the plasma performance for microelectronics applications. However, only a few researches have been carried out on the bias effect in an ICP discharge with a pulsed bias, and the plasma characteristics are still not well understood. Therefore, in this work, the so called Multiphysics Analysis for Plasma Soures-ICP (MAPS-ICP) solver has been employed to investigate the influence of the pulsed bias on the inductive nitrogen discharge behavior. The aim of this work is to elucidate the influence of the bias on the plasma characteristics, which is important for the improvement of the LPIII process.

This paper is organized as follows. In Section 2, the fluid model and the reaction set, together with the boundary conditions, are described. The effect of the pulsed bias on the plasma characteristics is shown in Section 3. Finally, a summary is given in Section 4.

2. Description of the fluid model

A schematic of the ICP reactor with a pulsed bias, studied in this work, is shown in Fig. 1. The nitrogen plasma is generated by a four-turn coil with radial positions at $r = 3$ cm, 5 cm, 7 cm, and 9 cm, respectively. The bottom electrode with a radius of 8 cm is fixed at a distance of 7 cm from the quartz window, and it is biased by a pulsed power to accelerate the positive ions towards the substrate. An insulator ring with a thickness of 1 cm is clamped around the substrate, and it is surrounded by a grounded thin metal layer.[21]

MAPS is a comprehensive modeling platform developed by Wang and his group for the multiphysics analysis of various plasma sources. It includes two solvers: the MAPS-CCP solver and the MAPS-ICP solver. This modeling platform has been used to simulation the ICP and capacitive coupled plasma (CCP) discharges.[22–28] The fluid model of the MAPS-ICP employed in this work is similar to that described in Refs. [24]–[26]. Therefore, only a brief description is included here.

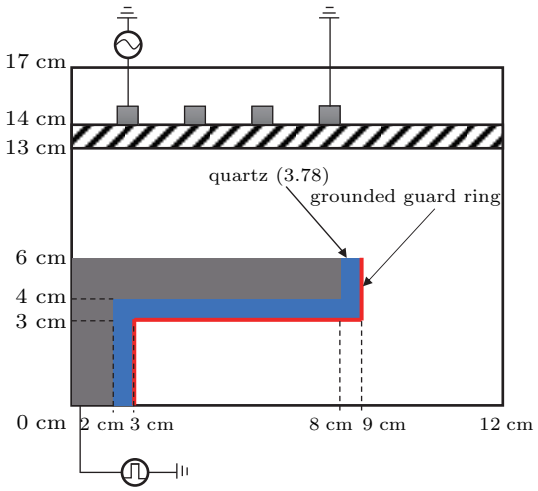


Fig. 1. (color online) Schematic diagram of the ICP immersion ion implantation instrument.

2.1. Plasma module

The fluid equations for electrons are as follows:

$$\frac{\partial n_e}{\partial t} + \nabla \cdot \boldsymbol{\Gamma}_e = S_e, \tag{1}$$

$$\boldsymbol{\Gamma}_e = -\frac{\nabla (n_e k T_e)}{m_e \nu_{en}} - \frac{e n_e}{m_e \nu_{en}} \boldsymbol{E}_s, \tag{2}$$

$$\frac{\partial}{\partial t}\left(\frac{3}{2} n_e k T_e\right) = -\nabla \cdot \boldsymbol{q}_e - e\boldsymbol{\Gamma}_e \cdot \boldsymbol{E}_s - E_e + P_{ind}. \tag{3}$$

Here, by ignoring the inertia term of the electron momentum equation, the electron flux $\boldsymbol{\Gamma}_e$ is presented in the drift-diffusion approximation form. S_e is the source term of electrons; n_e, T_e, m_e, and $\boldsymbol{q}_e$ are the density, temperature, mass, and energy flux of electrons, respectively; ν_{en} is the elastic collision frequency between electrons and neutrals; $\boldsymbol{E}_s$ is the electrostatic field; E_e is the energy transfer of electrons by collisions with other species; k is the Boltzmann constant; the period averaged inductive power deposition P_{ind} is described as $P_{ind} = 1/T \int_0^T J_\theta E_\theta \, dt$, where T is the period of the coil current, J_θ and E_θ are the azimuthal electron flux and the electric field.

Since the ions are assumed to be at room temperature, only the continuity and momentum equations are needed,

$$\frac{\partial n_i}{\partial t} + \nabla \cdot \boldsymbol{\Gamma}_i = S_i, \tag{4}$$

$$\frac{\partial n_i m_i \boldsymbol{u}_i}{\partial t} + \nabla \cdot (n_i m_i \boldsymbol{u}_i \boldsymbol{u}_i) = -kT_i \nabla n_i + e n_i \boldsymbol{E}_s + \boldsymbol{M}_i, \tag{5}$$

where n_i, Γ_i, m_i, and $\boldsymbol{u}_i$ are the ion density, flux, mass, and velocity, respectively. $\boldsymbol{M}_i$ represents the transfer of momentum from the ions by collisions with other species.

For the neutral species, the continuity equation is expressed as

$$\frac{\partial n_n}{\partial t} + \nabla \cdot (-D_n \nabla n_n) = S_n, \tag{6}$$

where n_n, D_n, and S_n are the density, diffusion coefficient, and source term of neutral species, respectively.

The gradients of the ion density and ion velocity at the boundaries are set to zero, i.e., $\nabla n_{\rm i} = 0$, $\nabla \boldsymbol{u}_{\rm i} = 0$. Since the secondary electron emission induced by the ion impact becomes important when a high negative voltage is applied to the substrate,[19,29] the boundary condition for the electron flux is

$$\boldsymbol{\Gamma}_{\rm e} = -(1-\Theta)\frac{n_{\rm e}}{4}\sqrt{\frac{8kT_{\rm e}}{\pi m_{\rm e}}} - \sum_i \gamma_i \boldsymbol{\Gamma}_i, \tag{7}$$

where $\Theta = 0.25$ is the reflection coefficient of electrons.[30] The secondary electron emission coefficient γ_i at the surface of the substrate is expressed as a function of the incident ion energy[19]

$$\begin{aligned} &\gamma_i(E_i) = \gamma_0, \ \ E_i < E_0, \\ &\gamma_i(E_i) = \gamma_0 + \frac{{\rm d}\gamma_i}{{\rm d}E_i}(E_i - E_0), \ \ E_i \geq E_0, \end{aligned} \tag{8}$$

where $\gamma_0 = 0.15$ is the secondary electron emission coefficient when the incident ion energy is below $E_0 = 3000$ eV, and ${\rm d}\gamma_i/{\rm d}E_i = 0.75 \times 10^{-3}$ eV^{-1} is adopted, for higher ion energy.

The continuity and energy equations for electrons are discretized by the finite volume method in space and the Crank–Nicolson scheme in time,[31,32] and the electron flux is solved by the first-order upwind scheme. The flux-corrected transport method is used to solve the ion equations.[33]

2.2. Electromagnetic module

The electrostatic field $\boldsymbol{E}_{\rm s}$ due to the space charge within the plasma is determined by solving the Poisson equation

$$\nabla^2 \phi(r,z) = -\frac{e}{\varepsilon_0}\left(\sum_i Z_i n_i - n_{\rm e}\right), \tag{9}$$

where ε_0 is the permittivity of free space.

The spatial–temporal distributions of the electromagnetic fields are obtained by solving the Maxwell equations,

$$\nabla \times \boldsymbol{E} = -\frac{\partial \boldsymbol{B}}{\partial t}, \tag{10}$$

$$\nabla \times \boldsymbol{B} = \mu_0 \boldsymbol{J} + \varepsilon_0 \varepsilon_{\rm r} \mu_0 \frac{\partial \boldsymbol{E}}{\partial t}, \tag{11}$$

where $\boldsymbol{E}$ is the electric field, $\boldsymbol{B}$ is the magnetic field, μ_0 is the vacuum permeability, and $\varepsilon_{\rm r}$ represents the relative dielectric constant of the dielectric window.

The plasma current $\boldsymbol{J}$ is given by

$$\frac{\partial \boldsymbol{J}}{\partial t} = \frac{n_{\rm e} e^2}{m_{\rm e}}\boldsymbol{E} - \nu_{\rm en}\boldsymbol{J}, \tag{12}$$

and it is set to zero in the vacuum and dielectric window regions.

The radial magnetic field at the interface of the dielectric window and vacuum is $B_r|_{\rm vac} - B_r|_{\rm die} = \mu_0 \alpha_\theta$, where α_θ is the current density. At the interface of the dielectric window and plasma region, the radial magnetic field and the azimuthal electric field are continuous.

The successive-over-relaxation method is applied to solve the Poisson equation, and the Maxwell equations are solved with the finite difference time domain (FDTD) method.[34]

Table 1. The reactions for the N_2 plasma taken into account in the model.

Reactions	Rate coefficient[b,c]	ε[d]	Ref.
$e + N_2 \rightarrow N_2 + e$	$1.04 \times 10^{-7}(T_e)^{0.43}\exp(-0.206/T_e)$ cm^3/s		[36]
$e + N \rightarrow N^+ + 2e$	a	4.54	[37]
$e + N_2^+ \rightarrow N + N$	$1.9 \times 10^{-9}(T_e)^{-0.3}$ cm^3/s		[43]
$e + N_2 \rightarrow N_2^+ + 2e$	$7.76 \times 10^{-9}(T_e)^{0.79}\exp(-16.75/T_e)$ cm^3/s	15.6	[36]
$e + N_2 \rightarrow e + 2N$	$2.15 \times 10^{-8}\exp(-14.39/T_e)$ cm^3/s	9.75	[39], [40]
$e + N_2 \rightarrow e + N_2(A)$	a	6.17	[38]
$e + N_2 \rightarrow e + N_2(B)$	a	7.35	[38]
$e + N_2 \rightarrow e + N_2(a')$	a	8.4	[38]
$N_2 + N_2(a') \rightarrow N_2 + N_2(B)$	1.9×10^{-13} cm^3/s		[35]
$N_2(A) + N_2(A) \rightarrow N_2 + N_2(B)$	7.7×10^{-11} cm^3/s		[35]
$N_2 + N_2(B) \rightarrow N_2 + N_2$	1.5×10^{-12} cm^3/s		[41]
$N_2 + N_2(B) \rightarrow N_2 + N_2(A)$	2.85×10^{-11} cm^3/s		[41]
$N^+ + N_2 \rightarrow N_2^+ + N$	4.45×10^{-10} cm^3/s		[35]
$N_2^+ + N \rightarrow N^+ + N_2$	$7.21 \times 10^{-13}\exp(T_{\rm gas}/300)$ cm^3/s		[42]
$N + N_2(A) \rightarrow N_2 + N$	2.0×10^{-12} cm^3/s		[42]
$N_2(a') + N_2(a') \rightarrow N_2 + N_2^+ + e$	$0.1 \times 5.0 \times 10^{-11}$ cm^3/s		[35]
$N_2(A) + N_2 \rightarrow N_2 + N_2$	3.0×10^{-18} cm^3/s		[43]
$N_2(A) + N_2(a') \rightarrow N_2 + N_2^+ + e$	1.0×10^{-12} cm^3/s		[35]
$N + N + N_2 \rightarrow N_2(B) + N_2$	$8.27 \times 10^{-31}\exp(500/T_{\rm gas})$ cm^6/s		[35]
$N + N + N \rightarrow N_2 + N$	1.0×10^{-29} cm^6/s		[43]
$N_2(B) \rightarrow N_2(A) + h\nu$	2.0×10^5 s^{-1}		[35]

[a] The rate coefficient is calculated from the corresponding collision cross section, and its unit is cm^3/s.
[b] $T_{\rm gas}$ is the room temperature.
[c] The unit of T_e is eV.
[d] ε is the threshold energy in eV.

The chemical reactions taken into account in the model are listed in Table 1. For ions, only N_2^+ and N^+ are included, because their densities are much higher than other ions, such as N_3^+ and N_4^+.[35] Besides, the ground-state N atoms, as well as three excited levels of N_2 molecules, i.e., $N_2(A)\left(A^3\Sigma_u^+\right)$, $N_2(B)\left(B^3\prod_g\right)$, and $N_2(a')\left(a'^1\Sigma_u^-\right)$, are also considered in this model.

3. Results and discussion

In this section, the influence of the pulsed bias on the inductively coupled nitrogen discharge has been investigated at a fixed ICP current of 16 A and an RF frequency of 10 MHz. The simulations are performed at a pressure of 10 mTorr. For the base case, the frequency and duty cycle of the pulsed bias is 8 kHz and 40%, respectively, and the waveform is shown in Fig. 2.[44]

$$V(t)=\begin{cases} V_0 t/t_{\rm r}, & 0<t<t_{\rm r}, \\ V_0, & t_{\rm r}<t<t_{\rm r}+t_{\rm p}, \\ V_0(t_{\rm t}-t)/t_{\rm f}, & t_{\rm r}+t_{\rm p}<t<t_{\rm t}, \\ 0, & t_{\rm t}<t<t_{\rm total}, \end{cases} \tag{13}$$

where $t_{\rm t}=t_{\rm r}+t_{\rm p}+t_{\rm f}$, $t_{\rm r}=4$ μs is the rise time, $t_{\rm p}=42$ μs is the plateau time, $t_{\rm f}=4$ μs is the fall time, and the power-off time is $t_{\rm totoal}-t_{\rm t}=75$ μs. The voltage of the pulsed bias varies from 0 V to −4000 V.

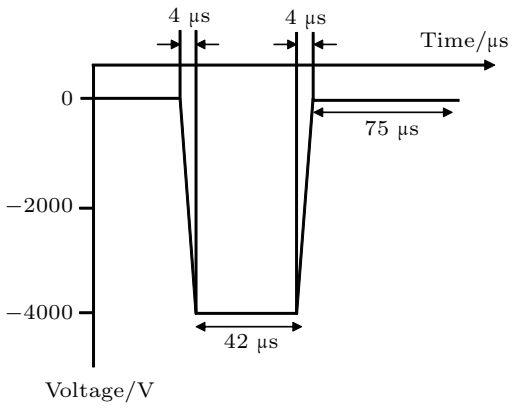


Fig. 2. Schematic of the pulsed voltage waveform.

3.1. Pulsed bias voltage effect

In the nitrogen LPIII process, the N^+ ions have an important influence on the implantation depth due to their high energy. Since the N_2^+ ions can recombine with electrons and then produce two nitrogen atoms, they are responsible for the high nitrogen atom concentration in the implanted sample. Therefore, it is of significant importance to understand the behavior of the ions and their ratio in the discharge. The evolutions of the N^+ ion density at the reactor center ($r=0$ cm, $z=9.5$ cm) and at the substrate surface ($r=0$ cm, $z=6$ cm), for various bias voltages, are presented in Fig. 3. When the bias power is turned on, the N^+ ion density at the reactor center increases rapidly, and then it reaches the steady state, as shown in Fig. 3(a). When the bias power is turned off, the N^+ ion density at the reactor center decays to a very low value in a short time. The evolution of the N^+ ion density at the substrate surface is similar to that at the reactor center, except that the ion density first increases to a peak value, and then it decays to a lower value at the beginning of the after-flow period (see Fig. 3(b)). This peak can be explained by the fact that when the pulse power is off, electrons move rapidly to the substrate, and the sheath region becomes thin. Therefore, the bulk plasma region is closer to the substrate, and more ions move to the substrate. Moreover, the secondary electron emission becomes less pronounced, hence the ion consumption due to the recombination is limited, and this is also attributed to the increase of the ion density at the substrate. In addition, the N^+ ion density increases significantly when the bias voltage varies from 0 V to −4000 V, both at the reactor center and at the substrate surface. This is because the plasma is heated not only by the inductive field, but also by the capacitive field caused by the pulsed bias. Therefore, the electrons gain more energy from the bias power, and this gives rise to the enhanced ionization.

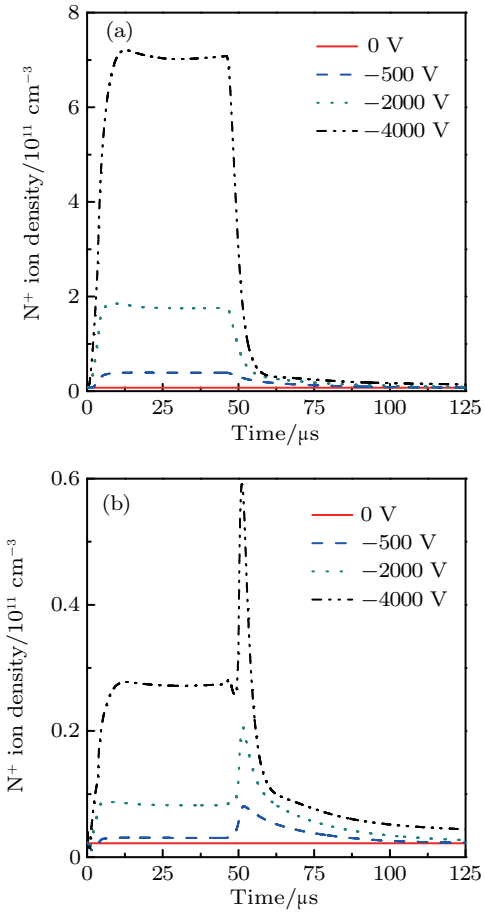


Fig. 3. (color online) N^+ ion density (a) at the reactor center, (b) at the substrate surface, as a function of time for various bias voltages for a pulse frequency of 8 kHz and duty cycle of 40%, in an ICP nitrogen discharge sustained at a current of 16 A and 10 MHz.

The N_2^+ ion densities at the reactor center and substrate surface as a function of time for different pulse voltages are shown in Figs. 4(a) and 4(b). The evolution of the N_2^+ ion density with time is similar to that of the N^+ ion density, except that the N_2^+ ion density at the steady state is about three times higher than the N^+ ion density. Compared to the N^+ ion density, the peak of the N_2^+ ion density at the beginning of the pulse-off period appears at a later time (i.e., 52.6 μs for the N_2^+ ion density, and 51.1 μs for the N^+ ion density, see Figs. 4(b) and 3(b)). Moreover, the N_2^+ ion density increases slower to the steady state at the beginning of the glow period, and similarly, the decay time of the N_2^+ density is also longer than the N^+ ion density. This indicates that the N^+ ions are more sensitive to the pulsed power than the N_2^+ ions. This is because the N_2^+ ions are mainly produced by the electron impact ionization of the feedstock N_2 gas, and the N^+ ions are mainly formed by the ionization of the N atoms. In this paper, we assume that the density of the feedstock is constant, which is because only a very small part of the background gas is ionized or excited at the low pressure, whereas the N atom density is modulated by the bias source. Therefore, the N^+ ion density exhibits a quicker response to the pulsed power.

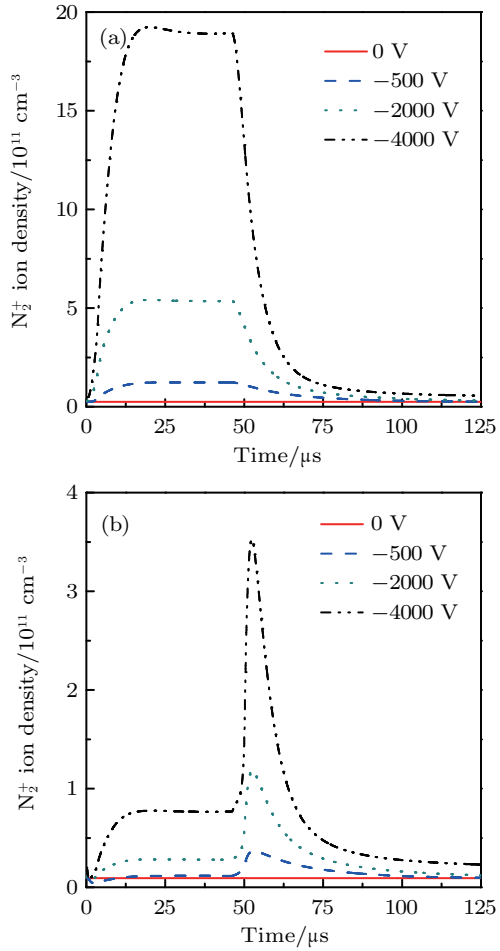


Fig. 4. (color online) N_2^+ ion density (a) at the reactor center, (b) at the substrate surface, as a function of time for various bias voltages for a pulse frequency of 8 kHz and duty cycle of 40%, in an ICP nitrogen discharge sustained at a current of 16 A and 10 MHz.

In order to understand the influence of the pulsed bias power on the electron heating, the spatiotemporal distributions of the inductive power density P_{ind} next to the reactor symmetry axis at different bias voltages for a whole pulse period are plotted in Fig. 5. In a pure inductive discharge without the pulsed bias source, the electrons are heated only by the inductive azimuthal electric field, and hence the inductive power density is very low (i.e., at maximum about 7.4×10^{-6} kW/cm^3, see Fig. 5(a)), leading to lower plasma densities (see Figs. 3 and 4). At the bias voltage of −500 V, the inductive power density during the power-on time (i.e., 0–50 μs) increases remarkably (i.e., at maximum about 36.3×10^{-6} kW/cm^3), which is about five times higher than that during the power-off period. This is because during the glow period, the electrons gain more energy from the capacitive electric field induced by the bias power. Therefore, the plasma density and the azimuthal electron flux increase considerably, which gives rise to the higher P_{ind} (see Fig. 5(b)). When the pulsed bias voltage is equal to −2000 V and −4000 V (see Figs. 5(c) and 5(d)), a higher power density during the pulse-on time is observed, which is again due to the higher azimuthal electron flux. Moreover, the inductive power density during the off period also becomes higher (i.e., at maximum about 17×10^{-6} kW/cm^3 at a bias voltage of −4000 V).

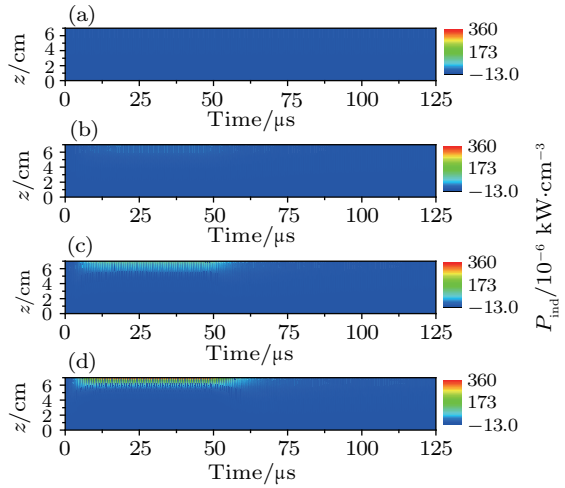


Fig. 5. (color online) Spatiotemporal distributions of the inductive power density next to the reactor symmetry axis at different bias voltages: (a) 0 V, (b) −500 V, (c) −2000 V, and (d) −4000 V, for a pulse frequency of 8 kHz and duty cycle of 40%, in an ICP nitrogen discharge sustained at a current of 16 A and 10 MHz.

Ratios of the N^+ and N_2^+ ion densities to the total ion density at the surface of the substrate as a function of time for various bias voltages are shown in Fig. 6. It is clear that the N_2^+ fraction is much higher than the N^+ fraction in the case without a bias power, i.e., $N_2^+/N^+ = 4.1$. When the bias power is applied to the substrate, the N^+ fraction increases rapidly to a maximum at the beginning of the power-on time, and then it decreases and reaches the steady state at the end of the glow

period. However, the N_2^+ fraction first decreases to its minimum, and then it increases to the steady state. When the bias power is turned off, the N^+ fraction drops rapidly to its minimum, and at a later time, it increases to the steady state. However, a reverse behavior of the N_2^+ fraction is observed. This is because when the bias power is turned on, the N^+ ion density increases faster than the N_2^+ ion density, so the N^+ fraction reaches its maximum in about 10 μs. At a later time during the glow period, the N^+ ion density keeps constant, whereas the N_2^+ ion density increases till about 19 μs (see Fig. 4(b)). This gives rise to a decrease in the N^+ fraction and an increase in the N_2^+ fraction. When both the N^+ and N_2^+ ion densities reach the steady state, i.e., after about 25 μs, the fractions of the N^+ and N_2^+ ions become constant. The minimum of the N^+ fraction and the maximum of the N_2^+ fraction at the beginning of the after-glow are again due to the quick response of the N^+ ions. Moreover, during the power-on time, the N^+ fraction becomes higher when the bias voltage increases from 0 V to −4000 V, whereas the N_2^+ fraction decreases with the bias voltage. This is because the N^+ ion density rises more rapidly (i.e., from 0.02×10^{11} cm^{-3} at 0 V to 0.27×10^{11} cm^{-3} at −4000 V, see Fig. 3(b)) than the N_2^+ ion density (i.e., from 0.09×10^{11} cm^{-3} at 0 V to 0.77×10^{11} cm^{-3} at −4000 V, see Fig. 4(b)). However, when the pulsed power is turned off, the N^+ fraction decreases with the bias voltage, whereas the N_2^+ fraction exhibits an increased trend due to a similar reason. These phenomena are similar to that observed in Refs. [45] and [46], i.e., the N^+ ion density increases faster with the RF power than the N_2^+ ion density.

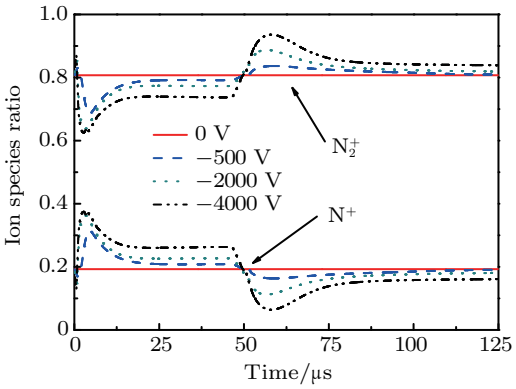


Fig. 6. (color online) Ratios of the N^+ and N_2^+ ion densities to the total ion density, as a function of time for various bias voltages for a pulse frequency of 8 kHz and duty cycle of 40%, in an ICP nitrogen discharge sustained at a current of 16 A and 10 MHz.

The radial distributions of the total ion flux at the substrate surface for various bias voltages averaged over one pulse period are shown in Fig. 7. The total ion flux is characterized by a center high profile at all selected bias voltages, and the ion flux above the substrate increases significantly with the bias voltage due to the high plasma density (see Figs. 3(b) and 4(b)).

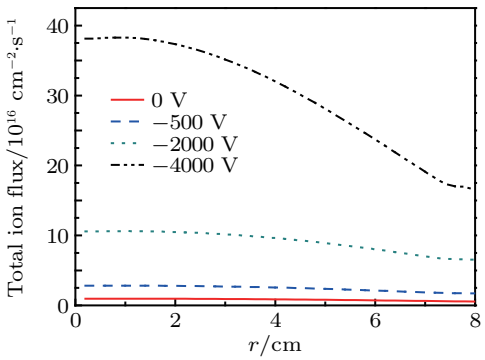


Fig. 7. (color online) Radial distributions of the total ion flux at the substrate surface averaged over one pulse period, for various bias voltages for a pulse frequency of 8 kHz and duty cycle of 40%, in an ICP nitrogen discharge sustained at a current of 16 A and 10 MHz.

3.2. The pulse frequency effect

For a better understanding of the pulsed bias effect on the nitrogen RF discharge properties, the calculations are performed for pulse frequencies of 8 kHz, 16 kHz, 25 kHz, and 40 kHz, at a duty cycle of 40% and a bias voltage of −2000 V. Since the behavior of the N^+ ion density during one pulse cycle is similar to the N_2^+ ion density, only the evolutions of the N_2^+ ion density at the reactor center and at the substrate surface are shown here. At the pulse frequency of 25 kHz and 40 kHz, the power-on time is only 16 μs and 10 μs, which is insufficient for the ions to achieve the steady state. Therefore, the N_2^+ ion density at the reactor center increases to its peak value at the end of the glow period, and then it decreases when the power is turned off, as shown in Fig. 8(a). Note the N_2^+ ion density at the substrate surface has a significant decrease at the beginning of the glow period, especially at higher pulse frequencies (see Fig. 8(b)). This is because during the ramp-up period, although the total power deposition increases with bias voltages, the bias power dissipation caused by the ion acceleration is more dominant, especially in the sheath region where the capacitive field is very strong, and this gives rise to a considerable decrease in the plasma density. As the bias voltage increases further, the electrons gain more energy from the higher capacitive bias power, and therefore, these energetic electrons enhance the plasma generation. Moreover, at higher pulse frequencies, the plasma density could not decay to a very low value in the limited after-glow period. Therefore, the average electron energy at the beginning of the glow period is low, which limits the ionization process, and leads to a more rapid decrease in the N_2^+ ion density. When the pulse frequency is lower than 16 kHz (i.e., with a power on time of 25 μs), the N_2^+ ion density can reach the steady state, and a peak value appears at the beginning of the after-glow period, which is similar to that shown in Fig. 4.

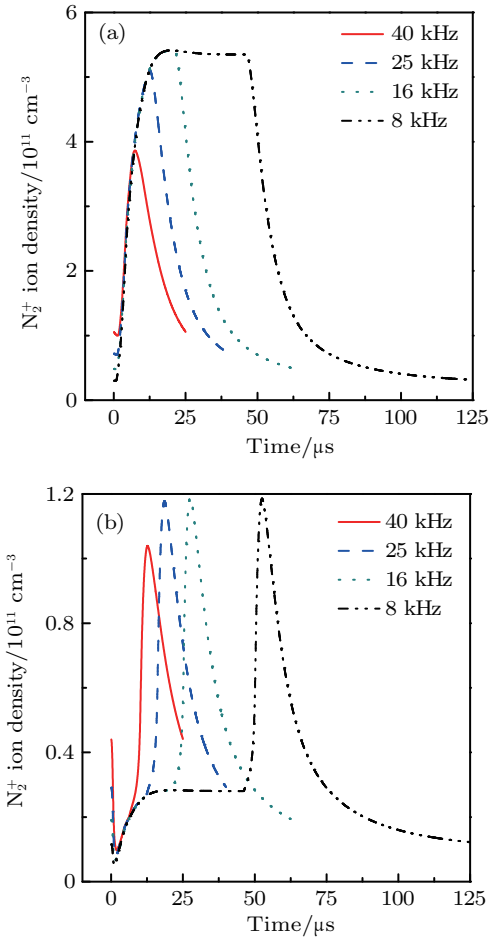


Fig. 8. (color online) N_2^+ ion density (a) at the reactor center, (b) at the substrate surface, as a function of time for various pulse frequencies for a bias voltage of −2000 V and duty cycle of 40%, in an ICP nitrogen discharge sustained at a current of 16 A and 10 MHz.

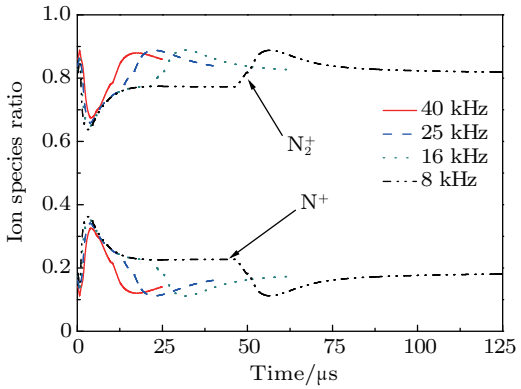


Fig. 9. (color online) Ratios of the N^+ and N_2^+ ion densities to the total ion density, as a function of time for various pulse frequencies for a bias voltage of −2000 V and duty cycle of 40%, in an ICP nitrogen discharge sustained at a current of 16 A and 10 MHz.

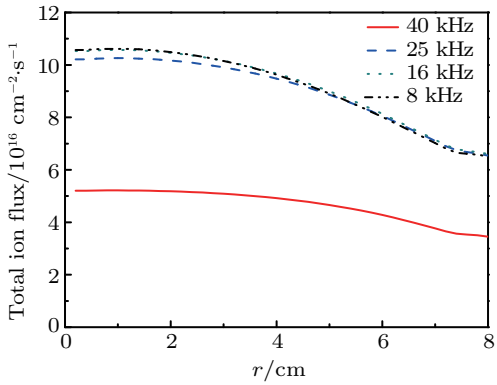


Fig. 10. (color online) Radial distributions of the total ion flux at the substrate surface averaged over one pulse period, for various pulse frequencies for a bias voltage of −2000 V and duty cycle of 40%, in an ICP nitrogen discharge sustained at a current of 16 A and 10 MHz.

The influence of the pulse frequency on the ratios of the N^+ and N_2^+ ion densities to the total ion density is shown in Fig. 9. It is clear that at the beginning of the power-on time, the N^+ fraction decreases with pulse frequency. This can be attributed to the lower electron energy at higher pulse frequency at the beginning of the glow period. Since the N^+ ions are mainly formed by the ionization of the N atoms, and the N atom density decreases with pulse frequency due to the lower dissociation rate of N_2 caused by the lower electron energy, the N^+ fraction increases slower at higher pulse frequencies.

The influence of the pulse frequency on the total ion flux at the surface of the substrate is shown in Fig. 10. It is clear that the pulse frequency has no significant influence on the radial distribution of the total ion flux, i.e., a center-high profile is observed at all selected pulse frequencies. However, the absolute value of the total ion flux has a slight decrease at 25 kHz. When the pulse frequency increases to 40 kHz, a remarkable decrease is observed (i.e., maximum of about 10.6×10^{16} cm^{-2}·s^{-1} at 8 kHz and 5.2×10^{16} cm^{-2}·s^{-1} at 40 kHz). This is again because the steady state cannot be reached at higher pulse frequencies, and the ion density is lower.

4. Conclusions

In this paper, a 2D self-consistent fluid model is applied to investigate the influence of the pulsed bias power on the nitrogen inductively coupled discharge for various pulse voltages and pulse frequencies.

From the simulation results, it can be found that the plasma density increases with bias voltage due to the heating of the capacitive field caused by the pulsed bias, and accordingly, the higher azimuthal electron flux leads to the higher inductive power density. The ion density at the substrate surface exhibits a peak at the beginning of the after-glow period due to a thin sheath and the reduction of the secondary electrons. The N^+ fraction shows a maximum at the beginning of the power-on time, and then it decreases and keeps constant. When the bias power is turned off, the N^+ fraction drops rapidly to its minimum, and at a later time, it increases to the steady state. Moreover, the N^+ fraction increases with the bias voltage during the power-on time, whereas the N_2^+ fraction exhibits a reverse behavior. The radial distribution of the axial total ion flux above the substrate is characterized by a center high profile, and the absolute value increases with the bias voltage.

We also found that the steady state cannot be obtained for higher pulse frequencies, i.e., 25 kHz and 40 kHz due to the shorter power-on time. In addition, the ion density at the substrate surface has a rapid decrease at the beginning of the glow period, especially at higher pulse frequencies. The maximum of the N^+ fraction at the beginning of the power-on time decreases with pulse frequency, and the minimum when the pulsed power is off at a pulse frequency of 40 kHz is slightly higher than those at lower pulse frequencies. The ion flux above the substrate becomes slightly lower at 25 kHz, and the decreasing trend becomes more evident at 40 kHz.

In conclusion, the plasma density and ion species ratio can be modulated by the bias voltage and pulse frequency. This is very important to realize, as it can help us to optimize the LPIII process.

References

[1] Husein I F, Chan C, Qin S and Chu P K 2000 *J. Phys. D: Appl. Phys.* **33** 2869
[2] Qin S and Chan C 1994 *J. Vac. Sci. Technol. B* **12** 962
[3] Qian X Y, Cheung N W, Lieberman M A, Current M I, Chu P K, Harrington W L, Magee C W and Botnick E M 1991 *Nucl. Instrum. Meth. Phys. Res. B* **55** 821
[4] Shao J, Jones E C and Chenug N W 1997 *Surf. Coat. Technol.* **93** 254
[5] Felch S B, Lee B S, Daryanani S L, Downey D F and Matyi R J 1998 *Mater. Chem. Phys.* **54** 37
[6] Tian X B, Zeng Z M, Tang B Y, Kwok T K and Chu P K 2000 *Surf. Coat. Technol.* **128** 226
[7] Tian X B, Zeng Z M, Zhang T, Tang B Y and Chu P K 2000 *Thin Solid Films* **366** 150
[8] Mukherjee S, Raole P M and John P I 2002 *Surf. Coat. Technol.* **157** 111
[9] Baumvol I J R, Krug C, Stedile F C, Green M L, Jacobson D C, Eagleshan D, Bernstein J D, Shao J, Denholm A S and Kellerman P L 1999 *Appl. Phys. Lett.* **74** 806
[10] Tian X B, Zeng Z M, Zeng X C, Tang B Y and Chu P K 2000 *J. Appl. Phys.* **88** 2221
[11] Mukherjee S and John P I 1997 *Surf. Coat. Technol.* **93** 188
[12] Chu P K, Qin S, Chan C, Cheung N W and Larson L A 1996 *Mater. Sci. Eng. R* **17** 207
[13] Mizuno B, Nakayama I, Takase M, Nakaoka H and Kubota M 1996 *Surf. Coat. Technol.* **85** 51
[14] Cheung N W 1994 *Nucl. Instrum. Meth. Phys. Res. B* **55** 811
[15] Qin S and McTeer A 2007 *Surf. Coat. Technol.* **201** 6759
[16] Qin S and McTeer A 2007 *Surf. Coat. Technol.* **201** 6508
[17] Valencia-Alvarado R, de la Piedad-Beneitez A, López-Callejas R, Barocio S R, Mercado-Cabrera A, Peña-Eguiluz R, Muñoz-Castro A E and de la Rosa-Vázquez J 2009 *Vacuum* **83** S264
[18] Agarwal A and Kushner M J 2005 *IEEE Trans. Plasma Sci.* **33** 252
[19] Agarwal A and Kushner M J 2007 *J. Appl. Phys.* **101** 063305
[20] Chang S J, Wu K Y, Yang Y H, Hwang J, Wu H Y, Pan R P, Lee A P and Kou C S 2007 *Thin Solid Films* **515** 8000
[21] Hebner G A and Miller P A 2000 *J. Appl. Phys.* **87** 7660
[22] Wang Y H, Liu W, Zhang Y R and Wang Y N 2015 *Chin. Phys. B* **24** 095203
[23] Liang Y S, Zhang Y R and Wang Y N 2016 *Chin. Phys. B* **25** 105206
[24] Sun X Y, Zhang Y R, Li X C and Wang Y N 2015 *Phys. Plasmas* **22** 053508
[25] Si X J, Zhao S X, Xu X, Bogaerts A and Wang Y N 2011 *Phys. Plasmas* **18** 033504
[26] Zhang Y R, Gao F, Li X C, Bogaerts A and Wang Y N 2015 *J. Vac. Sci. Technol. A* **33** 061303
[27] Wen D Q, Zhang Q Z, Jiang W, Song Y H, Bogaerts A and Wang Y N 2014 *J. Appl. Phys.* **115** 233303
[28] Liu W, Wen D Q, Zhao S X, Gao F and Wang Y N 2015 *Plasma Sources Sci. Technol.* **24** 025035
[29] Li X C and Wang Y N 2006 *Thin Solid Films* **506** 307
[30] Nitschke T E and Graves D B 1994 *J. Appl. Phys.* **76** 5646
[31] Hammond E P, Mahesh K and Moin P 2002 *J. Comput. Phys.* **176** 402
[32] Maday Y, Patera A T and Rønquist E M 1990 *J. Sci. Comput.* **5** 263
[33] Boris J P, Landsberg A M, Oran E S and Gardner J H 1993 *LCPFCT-Flux-corrected Transport Algorithm for Solving Generalized Continuity Equations*, NRL Memorandum Report No. 6410-93-7192
[34] Sun G and Trueman C W 2003 *Electron. Lett.* **39** 595
[35] Bogaerts A 2009 *Spectrochimica. Acta Part B* **64** 126
[36] Gudmundsson J T 2005 *Tech. Report* No. RH-09-2005
[37] http://www.lxcat.laplace.univ-tlse.fr/
[38] Itikawa Y 2006 *J. Phys. Chem. Ref. Data* **35** 31
[39] Liang Y S, Liu Y X, Zhang Y R and Wang Y N 2015 *J. Appl. Phys.* **117** 083301
[40] Cosby P C 1993 *J. Chem. Phys.* **98** 9544
[41] Guerra V and Loureiro J 1997 *Plasma Sources Sci. Technol.* **6** 361
[42] Levaton J, Amorim J, Souza A R, Franco D and Ricard A 2002 *J. Phys. D: Appl. Phys.* **35** 689
[43] Thorsteinsson E G and Gudmundsson J T 2009 *Plasma Sources Sci. Technol.* **18** 045001
[44] Stewart R A and Lieberman M A 1991 *J. Appl. Phys.* **70** 3481
[45] Kim G H, Rim G H and Nikiforov S A 2001 *Surf. Coat. Technol.* **136** 255
[46] Cho J, Han S, Lee Y, Kim O K, Kim G H, Kim Y W, Lim H and Suh M 2001 *Surf. Coat. Technol.* **136** 106